Chemical Engineering Journal 334 (2018) 2467–2479

Contents lists available at ScienceDirect

Chemical Engineering Journal

journal homepage: www.elsevier.com/locate/cej

Streamer propagation in a packed bed plasma reactor for plasma catalysis applications

Weizong Wang[a,*], Hyun-Ha Kim[b], Koen Van Laer[a], Annemie Bogaerts[a]

[a] Research group PLASMANT, Department of Chemistry, University of Antwerp, Universiteitsplein 1, BE-2610 Wilrijk-Antwerp, Belgium
[b] National Institute of Advanced Industrial Science and Technology (AIST), 16-1 Onogawa, Tsukuba, Ibaraki 305-8569, Japan

GRAPHICAL ABSTRACT

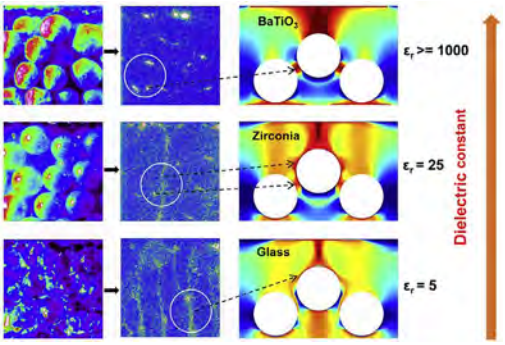

ARTICLE INFO

Keywords:
Plasma catalysis
Fluid simulation
Microdischarge
Packing beads
Dielectric constant
Environmental applications

ABSTRACT

A packed bed dielectric barrier discharge (DBD) is widely used for plasma catalysis applications, but the exact plasma characteristics in between the packing beads are far from understood. Therefore, we study here these plasma characteristics by means of fluid modelling and experimental observations using ICCD imaging, for packing materials with different dielectric constants. Our study reveals that a packed bed DBD reactor in dry air at atmospheric pressure may show three types of discharges, i.e. positive restrikes, filamentary microdischarges, which can also be localized between two packing beads, and surface discharges (so-called surface ionization waves). Restrikes between the dielectric surfaces result in the formation of filamentary microdischarges, while surface charging creates electric field components parallel to the dielectric surfaces, leading to the formation of surface discharges. A transition in discharge mode occurs from surface discharges to local filamentary discharges between the packing beads when the dielectric constant of the packing rises from 5 to 1000. This may have implications for the efficiency of plasma catalytic gas treatment, because the catalyst activation may be limited by constraining the discharge to the contact points of the beads. The production of reactive species occurs most in the positive restrikes, the surface discharges and the local microdischarges in between the beads, and is less significant in the longer filamentary microdischarges. The faster streamer propagation and discharge development with higher dielectric constant of the packing beads leads to a faster production of reactive species. This study is of great interest for plasma catalysis, where packing beads with different dielectric constants are often used as supports for the catalytic materials. It allows us to better understand how different packing materials can influence the performance of packed bed plasma reactors for environmental applications.

* Corresponding author.
E-mail addresses: wangweizong@gmail.com (W. Wang), Annemie.bogaerts@uantwerpen.be (A. Bogaerts).

https://doi.org/10.1016/j.cej.2017.11.139
Received 30 September 2017; Received in revised form 9 November 2017; Accepted 21 November 2017
Available online 22 November 2017
1385-8947/ © 2017 Elsevier B.V. All rights reserved.

1. Introduction

Packed bed dielectric barrier discharge (DBD) plasma reactors are gaining increasing interest for plasma catalysis, for various environmental applications, such as air pollution control and greenhouse gas conversion [1–14]. Plasma catalysis is based on the integration of a plasma and a catalyst, for improved performance, such as higher energy efficiency and better product selectivity. A synergistic effect has often been reported in plasma catalysis, but it is rather complicated. A distinction has to be made between the dielectric effect, originating from the dielectric constant of the packing beads, and chemical catalytic effects, either due to the beads themselves or arising from the catalytically active coating on the beads. Both effects will take place at the same time. As a result, the plasma and catalyst influence each other during operation. On one hand, the reactive plasma species (i.e., ions, radicals, and excited species) affect the catalyst properties, such as its morphology or its work function [15,16]. On the other hand, the existence of the packing beads (catalyst) in the reactor changes the electric field distribution and hence the discharge behavior [17,18], which leads to changes in the plasma chemistry and in the plasma performance for environmental applications. The underlying effects of the packing on the plasma characteristics are, however, far from understood. One of the reasons is the difficulty to perform experiments in this type of plasmas, more specifically by optical diagnostics, due to blocking of the visual path by the packing material. Therefore, computer modelling can be very useful to obtain a better insight in the underlying mechanisms.

In the past, some simple models of plasma-catalyst have been developed. Chang and Takaki et al. first developed a 0D model for a N_2/NF_3/O_2/H_2 mixture, and later a time-averaged 1D model for a N_2 plasma, based on solving Poisson's equation and the transport equations [19,20]. Due to the 1D limitation, however, they simply assumed the void between the beads to be spherical. Kang et al. applied a 2D model to study the first 20 ns of the understood propagation of microdischarges in a DBD reactor with two stacked ferroelectric beads inside [20]. Russ et al. also used a 2D fluid model to simulate the formation of microdischarges in a packed bed DBD reactor operating in dry air with 500 ppm NO, limiting to a short one-directional discharge with constant applied potential [21]. More recently, some more sophisticated 2D models were developed. Although not directly applied to a packed bed reactor, Babaeva et al. performed very relevant modelling work on the influence of dielectric spheres blocking a plasma streamer, by means of a 2D fluid model in humid air [22]. Kruszelnicki et al. studied the propagation of negative electrical discharges in a packed bed reactor without dielectric layer between the electrodes, using a combination of 2D fluid modelling and a purpose-built experimental setup [23]. The authors showed that surface ionization waves (SIWs) and positive restrikes are mainly responsible for reactive species production. Zhang et al. applied a 2D particle-in-cell/Monte Carlo collision (PIC/MCC) model to describe the filamentary discharge behavior in a packed bed DBD reactor in air [24].

In recent years, Van Laer and Bogaerts developed two complementary 2D axisymmetric fluid models, i.e., a so-called "contact point model" and a "channel of voids model", to mimic these two important features of a 3D packed bed reactor [25]. The "channel of voids model" was found to be crucial to capture all relevant plasma features, so it was subsequently also applied to study the effect of the dielectric constant of the beads in a microgap and mm-gap reactor [26], as well as the combined effect of bead size and dielectric constant of the beads [27]. These models were developed in helium. The reason was twofold: (i) helium yields a homogeneous discharge in DBD reactors, which is most easily described by a fluid model, and (ii) helium has a rather simple chemistry, thus reducing the calculation time, as this type of simulations is computationally very expensive due to severe mesh requirements [25].

However, for practical environmental applications, packed bed reactors (PBRs) are operated in molecular gases, such as air or CO_2 [1–14]. Molecular gases in general lack the ability to form a homogeneous plasma across the discharge gap, but they typically show a combination of streamer and surface discharges [23,28]. Therefore, in the present paper, we want to model a packed bed DBD reactor in air, focusing on the behavior of a streamer when it hits the packing material. We apply this model to dry air, for two reasons: (i) it still has a relatively small chemical reaction set, and (ii) to correctly simulate the propagation of the streamer, photoionization needs to be included, and this process is well described in literature for dry air [29,30].

Streamer propagation has been extensively studied in the past [22,23,31–35]. A few of these studies can be linked to plasma formation in a packed bed DBD reactor, as they discuss the influence of objects in the path of a streamer. Babaeva et al. studied the interaction of plasma filaments with objects blocking its path, such as dust particles [22,34,35]. Kruszelnicki et al. investigated the interaction of a negative electrical discharge with a 2D packed bed configuration of quartz rods, as mentioned above [23].

Besides modelling, ICCD imaging can also be very useful for gaining a better understanding in the plasma characteristics of a packed bed DBD reactor, although it is quite challenging due to the complex geometry. In the past, Kim et al. investigated the discharge phenomena in PBRs and identified two types of discharges, i.e., streamer-like surface discharges and local microdischarges between the packing beads (also called partial discharges) [36–40]. Tu et al. reported the transition from a typical filamentary discharge to a combination of local microdischarges and predominant surface discharges in a Ni/Al_2O_3 filled packed bed reactor [41]. Butterworth and Allen observed two main types of discharges in a single catalyst pellet DBD reactor using nitrogen, i.e., point-to-point local microdischarges and surface streamers, which are affected by the material dielectric constant [42]. These studies have thus revealed important features of both local microdischarges and surface discharges, but the underlying formation mechanisms of these discharges are far from understood.

In our paper, we therefore study in detail the streamer behavior, and more specifically for packing materials with different dielectric constants. Indeed, in practice different packing materials are used in packed bed DBD reactors for environmental applications, with dielectric constants varying from 5 (glass, quartz), over 9 (alumina), 25 (zirconia) and 100 (titania), up to 1000 and more (barium titanate). They often act as catalyst supports in plasma catalysis. A crucial research question is thus how the dielectric constant of the packing beads influences the plasma characteristics and the plasma-catalyst interactions. The choice of packing beads with appropriate dielectric constant is of prime importance, as it will affect the charging of the beads, and thus the electric field inside the plasma, and hence the streamer behavior in the vicinity of the catalyst surface, as well as the production of reactive species that are available for the catalytic reactions [43]. Thus, it influences the catalytic performance. Therefore, it is of uttermost importance to better understand how different packing materials can influence the performance of packed bed DBD reactors for plasma catalysis applications.

2. Description of the model

We used a 2D axisymmetric fluid model, with semi-kinetic description of the electrons, developed within COMSOL Multiphysics Simulation software [44]. The model is based on solving a set of coupled differential equations that express the conservation of mass, momentum and energy, for the different plasma species. In addition, the Poisson equation is solved, to self-consistently calculate the electric field distribution, using the densities of the different charged plasma species as input in the discharge gap, and solving for zero space charge in the dielectric material. The gas heating effect is not included in the simulation, because of the limited maximum molar fraction of electrons, i.e., around 10^{-4}. The energy exchange upon collision between

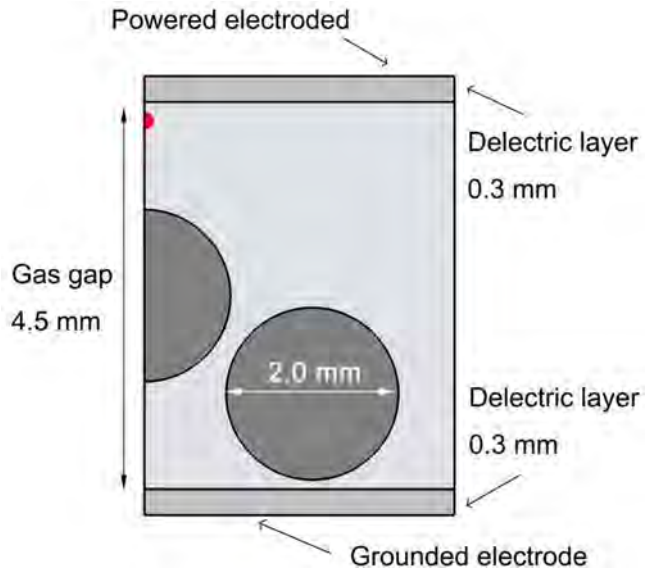

Fig. 1. 2D axisymmetric reactor geometry used in the model. The red dot indicates the location of initial enhanced electron density (see text). (For interpretation of the references to colour in this figure legend, the reader is referred to the web version of this article.)

electrons and neutrals, which would be the most important factor for gas heating in our case, is minor. Moreover, we only consider a short discharge period, shorter than 20 ns, so the energy accumulation is not very significant. Based on these considerations, for simplicity, we assume a constant gas temperature of 300 K. More details about this model can be found in [25]. As we focus here on the propagation of a streamer, photoionization needs to be included, which was not the case in [25]. For this purpose, we introduce three Helmholtz differential equations [30] (see details in Section 1 of the supporting information (SI)). The reactor geometry to which the model is applied will be explained in Section 2.1, while the chemistry considered in the model for dry air will be presented in Section 2.2.

2.1. Geometry

Modelling a packed bed DBD reactor in the entire 3D geometry would lead to extremely long calculation times, due to severe mesh requirements. Therefore, we consider a 2D representation, as presented in Fig. 1. The geometry consists of a powered electrode at the top and a grounded electrode at the bottom, both covered by a dielectric layer with 0.3 mm thickness. The gap between these dielectric layers is 4.5 mm. Note that packed-bed reactors can be constructed with or without dielectric layers between the packing beads and the electrodes. Packed-bed reactors with dielectric layers can achieve a higher removal efficiency and ozone yield and less byproducts [45]. Besides, from a practical perspective, utilizing a packed-bed reactor with dielectric layers avoids the occurrence of arcing. Therefore, in our simulations, we consider two dielectric layers covering both electrodes. Moreover, the pressure increase during operation is negligible and a constant pressure of 1 atm is assumed during the simulation.

Because we want to model the streamer propagation and its interaction with the packing, we make sure that the streamer has enough room to fully develop before hitting the surface of a packing bead, so we include some empty space near the top dielectric layer. We place the middle bead on the side of the symmetry axis, in order to make use of this symmetry axis, and to allow the streamer to be initiated directly above the middle bead on the symmetry axis.

Because we are interested in the behavior of a single streamer, we do not need to model multiple cycles of applied potential and we can focus here only on a few tens of nanoseconds, to cover the average lifetime of a plasma streamer in a DBD reactor. The streamer is artificially initiated just beneath the dielectric layer covering the powered electrode, by artificially increasing the electron density at 0.4 mm below the surface of the top dielectric layer to $10^{14}\,m^{-3}$. We apply a constant voltage of −10 kV at the top electrode, which is justified for this short time-scale, and this forces the (negative) streamer downwards. We consider packing beads with different dielectric constants, equal to 5 (glass, quartz; SiO_2), 9 (alumina; Al_2O_3), 25 (zirconia; ZrO_2), 100 (titania; TiO_2) and 1000 (barium titanate; $BaTiO_3$). It should be noted that $BaTiO_3$ can have a range of different dielectric constants, and the $BaTiO_3$ beads used in our experiments have $\varepsilon = 2600$ (see below). However, in our simulations we use $\varepsilon = 1000$, because a further increase in dielectric constant did not affect the results (e.g., no further enhancement of the electric field was observed), but the calculation time of the model with $\varepsilon = 2600$ is much longer than with $\varepsilon = 1000$ [26]. The reason why further increasing the dielectric constant (above 1000) of the packing materials does not change the results, such as the average electric field, is because the voltage distributed across the dielectric layer and the gas gap takes up almost all the applied voltage, and thus the voltage drop across the beads becomes negligible for very large dielectric constants. As a result, the enhancement factor of the electric field as a function of dielectric constant of the packing beads does not change with further increase of the dielectric constant. This has also been explained in [19]. The dielectric constant of the two dielectric layers covering the surface of the electrodes is 9 (alumina) in all simulations.

2.2. Plasma chemistry

We consider dry air as discharge gas, i.e., a mixture of 80% N_2 and 20% O_2. The plasma chemistry set contains 15 different species, namely molecular N_2 and O_2, atomic N and O, N_2^+, O_2^+ and O^+ ions, four N_2 electronically excited states (i.e., N_2 ($A^3\Sigma$), N_2 ($B^3\Pi$), N_2 ($C^3\Pi$) and N_2 ($a'^1\Sigma$)), one excited state of atomic O (O^1D), as well as NO, O_3 and the electrons. These species react with each other in 41 different reactions, which are listed in detail in the SI.

To correctly calculate the propagation of the streamer, we need to include extra equations to account for photoionization, as explained in the SI. In N_2-O_2 mixtures, photoionization occurs when O_2 molecules absorb photons, which are emitted as a result of the quenching of highly excited N_2 molecules from the singlet states $b^1\Pi$, $b'^1\Sigma_u^+$ and $c'_4{}^1\Sigma_u^+$. We refer to the SI for more details on how photoionization is included in the model. The transport coefficients of all the different species, i.e. the mobilities and diffusion coefficients, are adopted from literature [46,47].

Besides the reactions in the gas phase, we also included some surface reactions in the model, i.e., quenching of all the excited species and neutralization of the ions to their respective ground state molecule or atom. Upon neutralization, the ions are assumed to have a probability of 0.05 to emit a secondary electron with an energy of 5 eV.

3. Experimental setup

In order to provide qualitative comparison of the modes of discharge propagation, we also performed experiments to observe the plasma generation on the surface of various packing materials at atmospheric pressure. Four different non-porous packing materials (glass, alumina, zirconia, and $BaTiO_3$) have been tested to compare the effect of dielectric constant on the plasma generation in the packed bed reactor. A picture of the experimental setup is shown in Fig. 2. The experiment is carried out in a plate-to-plate packed bed reactor with a gap distance of 8 mm. An intensified charged coupled digital (ICCD) camera (Andor, iStar DH334T) allows to visualize the interaction between plasma and packing material. The upper electrode is connected to a negatively pulsed high voltage output (−10 kV) and the bottom electrode is grounded. The pulse rise time was about 20 ns, and the pulse

Fig. 2. Experimental configuration of the packed bed plasma reactor, used for ICCD imaging.

width was 300 ns (full width at half maximum; FWHM). The pulse frequency was fixed at 1 Hz for the ICCD imaging of the discharge. ICCD measurements were conducted with synthetic air (80% N_2 and 20% O_2), using a flow rate of 1 L/min. The discharge images were captured with a gate-time of 100 ns with full intensification. The images of packing materials without discharge were recorded with a 100 μs gate-time and 20% intensification.

4. Results and discussion

First we present in detail the streamer propagation for a packing with dielectric constant equal to 5 and 1000 (corresponding to SiO_2 and $BaTiO_3$, respectively). Subsequently, we explain the effect of the dielectric constant (in the range between 5 and 1000) on the discharge behavior, the occurrence of different discharge regimes, the time of discharge evolution, the propagation speed of streamer and surface ionization waves, and on the production of reactive species. We also compare with our experimental observations, and we discuss the results in terms of their relevance for environmental applications.

4.1. Streamer propagation for a packing with dielectric constant = 5

At the beginning of the simulation, when plasma is not yet formed, we can clearly observe the influence of the dielectric beads on the electric field, which is induced by the applied potential. Indeed, as is clear from Fig. 3, when an applied electric field is imposed on a solid dielectric immersed in a gas, the polarization of dielectric beads leads to a reduction of the electric field inside the dielectric relative to the electric field in the gas. The electric field strength is enhanced at the poles (top and bottom in this configuration), while electric field minima are formed in the middle, i.e., at the left and right of the beads, where the vector applied electric field is perpendicular to the surface normal. Where the beads are closest to each other, opposite charges are close, slightly increasing the electric field at these positions. This electric field distribution will have its influence on the propagation of the streamer, as presented below.

In Fig. 4 we show the evolution of the electron density over a simulated time of 12 ns. The electron temperature, as well as the electron impact ionization rate and the photoionization rate, which are responsible for this behavior (i.e., discharge development) are plotted in Figs. S1–S3 of the SI, while the net positive space charge is plotted in Fig. S4 of the SI.

In the beginning, only a slight maximum electron density (barely visible at the colour scale of Fig. 4) can be found right at the top of the

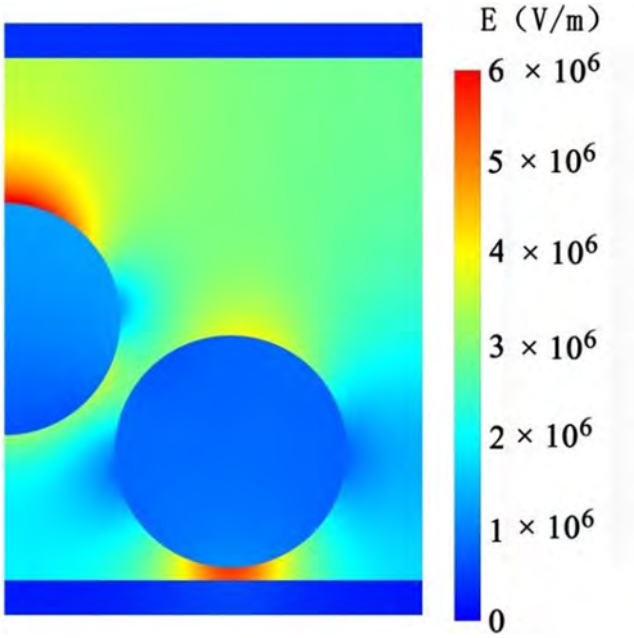

Fig. 3. Electric field distribution at the beginning of the simulation (0 ns), for a packing with $\varepsilon_r = 5$.

gas gap beneath the dielectric layer covering the powered electrode (i.e., cathode) (not shown), which arises from the artificially enhanced initial electron density (see Fig. 1 above). Upon application of the voltage, separation of charge in the initial plasma seed occurs-ions are accelerated towards and neutralize the cathode, while electrons accelerate downward. The electrons undergo a Townsend-like avalanche process by electron impact ionization of the background gases and a negative streamer forms, characterized by the negative space charge in the head of the streamer, followed by a quasi-neutral column. The electrons are moving downward at 2 ns, as indicated in Fig. 4. A slight increase in electron density can also be seen above the upper packing bead. The latter is caused by the enhanced electric field strength (see Fig. 3), which increases the electron temperature, and thus the electron impact ionization rate at the surface of the upper bead (see Figs. S1 and S2 in the SI).

In the next frame (3 ns), the streamer reaches the surface of the upper dielectric bead. The electric field enhancement at the poles of the top bead produces regions of high electron temperature and electron

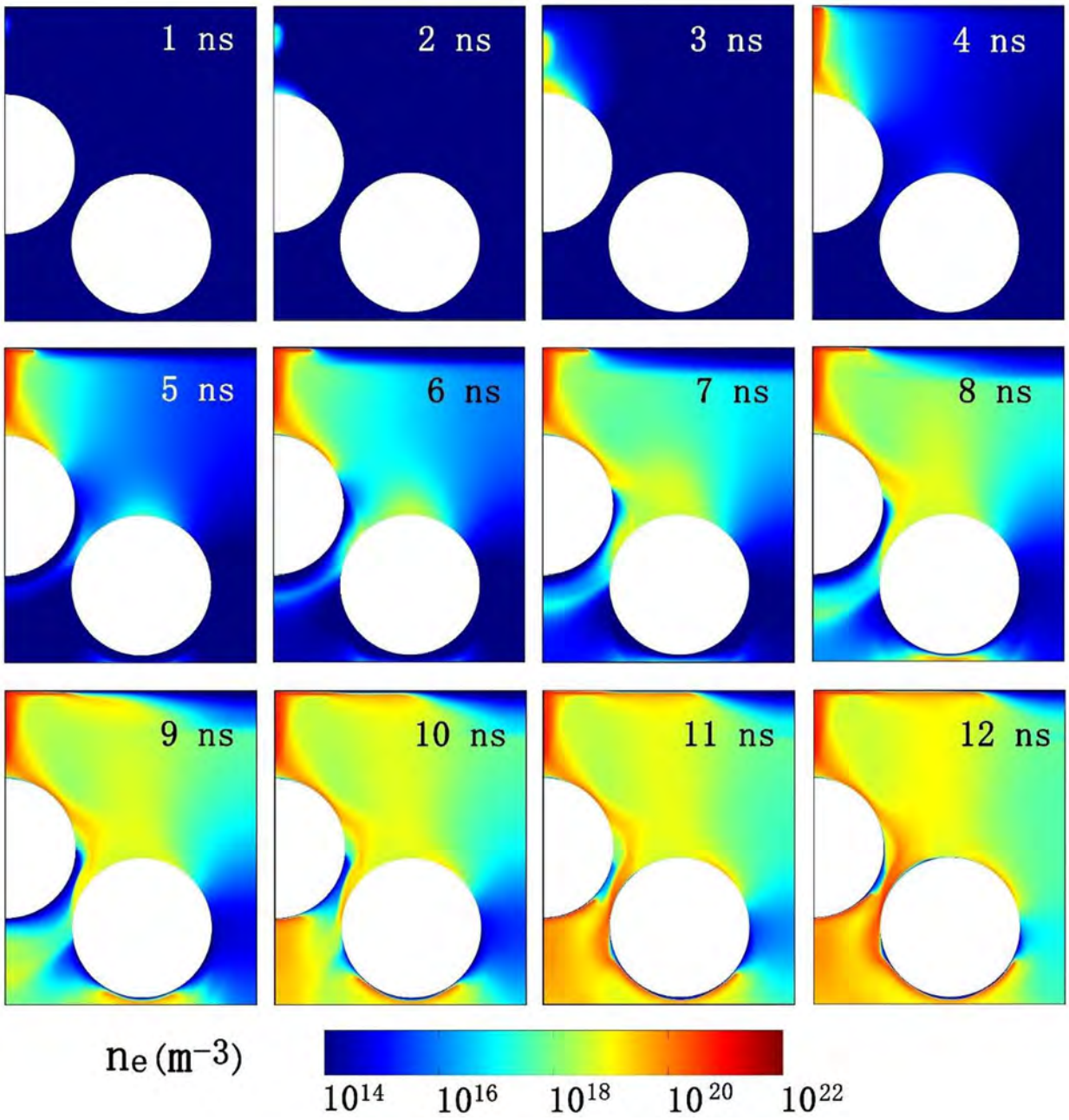

Fig. 4. Evolution of the electron number density distribution over 12 ns, for a packing with $\varepsilon_r = 5$.

impact ionization (see again Fig. S1 and S2 in the SI), which give rise to an instantaneous positive restrike. The latter has the characteristics of a positive streamer with a large positive space charge at its head, followed by a quasi-neutral column (see Fig. S4 in the SI). In the next frames (4–5 ns) we can see how the positive streamer is launched from the dielectric bead surface upward to the dielectric layer covering the cathode. With increasing electron number density due to electron impact ionization (see Fig. S2 in the SI), the potential difference between the cathode and the top dielectric bead collapses and the electron temperature in the central discharge channel drops rapidly (see Fig. S1 in the SI: 4–5 ns). Correspondingly, the electron impact ionization rate slightly drops, in spite of the high electron density.

With the streamer development, and thus the establishment of a conductive channel, photoionization gradually becomes more important, although its rate is still three orders of magnitude lower than the electron impact ionization rate (cf. Fig. S2 and S3 in the SI). It is worth mentioning that photoionization nevertheless plays a significant role in the discharge propagation, as it seeds the initial charge and promotes the discharge development in regions of high electric field, more specifically, regions that are difficult to access for electrons from the main streamer. Hence, it can initiate avalanches at remote locations and influence the streamer propagation speed. This is clearly indicated in Fig. S5 in the SI, which compares the electron number density distribution with and without including the photoionization effect.

After 5 ns, the discharge spreads out horizontally over the dielectric layer covering the cathode, caused by a so-called surface ionization wave [48]. The space charge that accumulates at the dielectric layer covering the cathode locally lowers the electric field strength. This results in lateral strong electric field differences at the surface of the dielectric layer, between the plasma region and the neutral gas region directly next to it. This difference initiates a surface ionization wave, which slowly expands the surface discharge over the dielectric layer (6–7 ns). The surface ionization wave is a so-called positive ionization wave, which is launched from the region of high electric field at the

edge of the surface ionization wave and has a high density of energetic electrons. The electron temperature at the head of the surface ionization wave is very high, i.e., above 6 eV, due to the very strong electric field in the lateral direction, and it decreases to around 1 eV in the conductive column behind this head (see Fig. S1 in the SI). The space charge separation and electric field enhancement in the head of the surface ionization wave produces a very high electron impact ionization rate of ca. $5 \times 10^{30}\,m^{-3}\,s^{-1}$ at 8 ns, as is shown in Fig. S2 in the SI. Also the photoionization rate shows a local maximum at the edge of the ionization wave, because of the very high electric field and electron temperature, producing many highly excited N_2 molecules, followed by quenching towards the formation of more photons.

During the development of this surface ionization wave, also called surface discharge, at the top dielectric surface, the electrons also charge the bead surface, again resulting in a lowering of the local electric field, and thus in a difference between the electric field at the top of the bead and the bead surface in its direct vicinity. This also results in a surface ionization wave on the bead surface (see Fig. 4; 5–6 ns). The original streamer has now converted to what is called a standing filamentary microdischarge [23,48], with a relatively narrow column of plasma between both dielectric materials, with on either surface wider "feet" of plasma (see Fig. 4; 6 ns).

As mentioned before, without the influence of plasma, i.e., just applying a potential difference, the electric field is enhanced at the top of the packing beads. This also occurs for the lower dielectric bead on the right. As a result, the electron temperature (Fig. S1 in the SI) and the electron impact ionization rate (Fig. S2 in the SI) are slightly enhanced locally at the top of this bead during the first 5–6 ns. With seed electrons coming from photoionization, produced by the photons emitted from the plasma nearby (Fig. S3 in the SI), some discharge can be formed on the surface of this lower dielectric bead (see Fig. 4; 6 ns). The lack of initial seeding through photoionization explains why avalanches between the packing beads and the bottom dielectric plate do not occur below 6 ns-this region is shadowed from the photoionizing radiation due to blocking by the dielectric beads.

From 7 to 8 ns, the surface discharge on the top dielectric bead on the left can link with the local discharge on top of the right lower bead, further spreading the plasma from the left bead to the top surface of the right bead (see Fig. 4). The plasma density directly above the lower bead will now also increase in the direction of the upper dielectric layer, due to drift of the ions. At around 10 ns this results in increased space charge at the dielectric layer directly above the lower packing bead (see Fig. 4).

Due to the presence of conductive plasma in the upper region of the reactor, starting from about 7 to 9 ns, the largest potential difference (and thus electric field) is now found in the lower region of the reactor, as is obvious from Fig. 5. Between the lower grounded electrode and the right bead, the electric field strength and hence the electron temperature becomes strong enough to cause a discharge, resulting in a local high electron impact ionization rate (see Fig. S2) and hence a visual plasma density in this region after 8 ns (see Fig. 4). However, the increased electric field strength and hence the electron temperature also cause an ionization wave to be sent out from the bottom surface of the left bead. Between 5 and 8 ns, it propagates away from the bead surface towards the grounded electrode. When it hits the dielectric covering the grounded electrode, a positive restrike is again formed, going upwards towards the bottom surface of the left packing bead, much like the behavior of the initial streamer starting at the top dielectric layer. When it reaches the bottom surface of the left bead, at around 10 ns, a surface ionization wave is again formed, now on the bottom of the left bead.

When the filamentary discharge channel between the bottom of the left bead and the bottom dielectric layer is established, the potential drop collapses, and thus the local electron temperature drops rapidly after 9 ns. Consequently, the electron impact ionization rate also slightly decreases. At the same time, due to the high electron density in the region surrounded by the two beads and the bottom dielectric layer

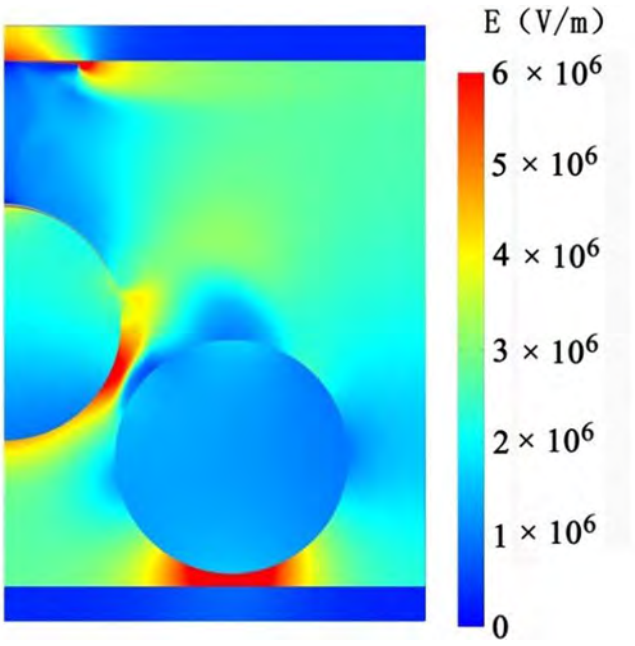

Fig. 5. Electric field distribution at 7 ns, for a packing with $\varepsilon_r = 5$.

at around 10 ns, the photoionization rate gradually increases (Fig. S3 in the SI). However, electron impact ionization still dominates over photoionization (cf. Figs. S2 and S3 in the SI). Finally, in between the two packing beads, where the electric field is enhanced in a packed bed reactor, the surface ionization wave can now jump towards the adjacent bead surface, and propagate further over its surface. The resulting discharge between the two packing beads can now also be seen as a local filamentary microdischarge, comparable to the earlier formed filaments between the beads and the upper or lower dielectric surface, but over a smaller distance (see 12 ns in Fig. 4).

Overall, our calculations reveal that the plasma in a packed bed DBD reactor with packing dielectric constant of 5 can manifest itself into three modalities-positive restrikes, filamentary microdischarges and surface ionization waves. Restrikes between the dielectrics result in the formation of filamentary microdischarges. Surface charging creates electric field components parallel to the dielectric surface, and leads to the formation of surface discharges or surface ionization waves. Surface discharges propagate on the bead surface and jump towards the adjacent bead, leading to the establishment of a standard filamentary microdischarge between the packing beads.

4.2. Streamer propagation for a packing with dielectric constant = 1000

To investigate the influence of higher dielectric constants of the packing beads on the discharge mechanism, we present in Fig. 6 the time evolution of the distribution of the electron number density, for a packing with dielectric constant of 1000 (characteristic for $BaTiO_3$). The corresponding distributions for the electron temperature, electron impact ionization rate and photoionization rate are plotted in Figs. S6–S8 of the SI.

After a Townsend-like avalanche process by electron impact ionization, an instantaneous positive restrike crosses the gas gap between the top surface of the left bead and the top dielectric layer at 1.5 ns. This behavior was also observed for a packing with $\varepsilon_r = 5$, but only after a much longer time of 4 ns (cf. Fig. 4). Indeed, the higher the dielectric constant of the packing, the stronger is the polarisation of the material, and thus, the greater is the difference between opposite charges at the closest distance between the packing and the dielectric layer, and between two packing beads. The electric field in these regions is thus enhanced for a packing with higher dielectric constant. As a result, the

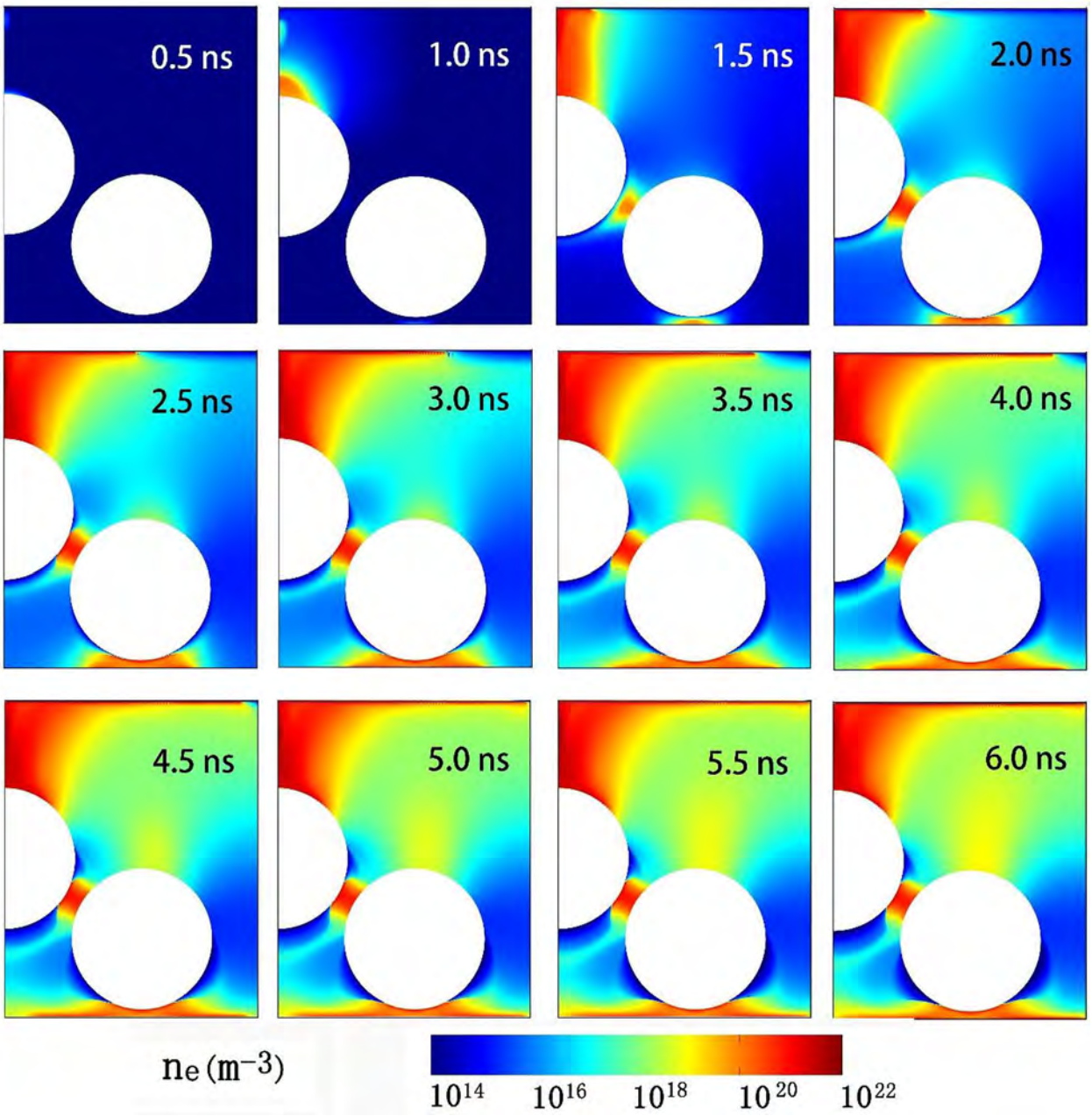

Fig. 6. Evolution of the electron number density distribution over 6 ns, for a packing with $\varepsilon_r = 1000$.

positive restrike occurs earlier in time than for a packing with $\varepsilon_r = 5$. Furthermore, at the same stage of discharge development, the electron temperature and hence the electron impact ionization rate, as well as the photoionization rate, are higher for larger dielectric constant of the packing beads (cf. the results at 1 ns in Figs. S6–S8 with those at 2 ns in Figs. S1–S3 of the SI). Correspondingly, the discharge channel diameter becomes wider (see Fig. 6; 1.5 ns). The filamentary discharge charges the top surface of the left bead, as well as the top dielectric layer, and reduces the adjacent electric field and electron temperature (see 1.5 ns in Fig. S6 in the SI). The electron impact ionization rate also slightly decreases, but it is less pronounced due to the high electron density (see 2 ns in Fig. S7 in the SI).

When the discharge channel between the top dielectric layer and the top surface of the left bead is established, the potential drop and thus the electric field in this gap are reduced, and the voltage is more distributed in the wider region between the packing beads and the dielectric layer, as well as between the two packing beads. Therefore, a microdischarge forms after the restrike of a positive streamer between the bottom surface of the right bead and the bottom dielectric layer (see Fig. 6; 2 ns). Almost at the same time, a local (or point-to-point) filamentary microdischarge takes place at the contact points between both packing beads, due to the electric field enhancement and hence the increased electron temperature and electron impact ionization rate. These microdischarges between the lower bead and the lower dielectric surface, as well as between both beads, happen much earlier in time than for the packing with $\varepsilon_r = 5$ (i.e., only around 9–12 ns; cf Fig. 4). This is caused by the larger dielectric constant of the packing materials, yielding a stronger polarisation of the beads. Meanwhile, the plasma charges the surface of the dielectric layer and packing beads, producing tangential components of the electric field, leading to surface ionization waves. The latter are most pronounced for the top and bottom dielectric layers (see Fig. 6: from 2 ns onwards). As mentioned in previous section, at the edge of the surface ionization waves, there is a very high electric field and hence a very high electron temperature, and thus also

a high electron impact ionization rate (see Figs. S6 and S7 in the SI). Therefore, the plasma continues to propagate gradually along the surface of the dielectric layers (see 2–6 ns in Fig. 6) due to electron transport (mainly migration in the electric field) as well as by photoionization, creating seed electrons in regions of high electric field (Fig. S8).

Note that the stronger polarization of the dielectric beads with $\varepsilon_r = 1000$ produces a stronger electric field enhancement at the poles of the beads. The higher electric field and hence electron impact ionization rate in the region above the top surface of the right packing bead gradually creates a second conductive channel towards the top dielectric layer (see 3–6 ns in Fig. 6), where the initial electrons were seeded by photoionization, produced by the photons emitted from the plasma nearby.

In summary, our calculations reveal that in a packed bed DBD reactor with packing dielectric constant of 1000 localized (point-to-point) filamentary microdischarges between the packing beads take place and no surface discharge propagation on the surface of the beads is observed.

4.3. Changing discharge behavior for packings with different dielectric constants

We showed in Section 4.1 for a packing with dielectric constant of 5 that when the surface ionization wave on the surface of the left bead propagates downwards and the conductive plasma channel on top of the right bead develops upwards, the surface ionization wave jumps towards the adjacent bead surface and establishes a discharge channel between the two beads (see Fig. 4; 7–12 ns). In contrast, for a packing with dielectric constant of 1000, the conductive channel between the two beads only manifests itself as a clearly defined local discharge at the contact points (see Fig. 6; between 2 and 6 ns). This is also referred to in literature as a point-to-point or polar discharge [42], or as partial discharges [36–40].

Hence, there is a transition in discharge mode from surface discharges to local filamentary discharges when the dielectric constant of the packing beads rises from 5 to 1000. For intermediate dielectric constants, a mixed mode of surface discharges and local discharges exists, as shown in Fig. 7 for packing beads with $\varepsilon_r = 100$. The same behavior was observed for $\varepsilon_r = 9$ and 25 as well. The plasma initiates in a local discharge mode between both packing beads (see 2–4 ns) which guides the passage of a surface ionization wave on the bead surface through the local discharge area (see 5–6 ns) and they merge at around 5.5 ns. Hence, surface discharges across the packing beads start to appear together with the local discharges. In other words, the local discharge at the contact point between adjacent beads can help promote the propagation of the surface discharges towards the next packing bead. This trend is in good agreement with experimental data by Kim et al. [40] obtained by time-resolved ICCD imaging of positive pulsed corona-induced surface streamers.

Our simulations were carried out for only two packing beads between both electrodes. However, we believe that if more packing beads would be present in the simulations, most of the conclusions will be the same, because most of them are qualitatively confirmed by our experiments, which were carried out with more beads (see next section).

It is however difficult to predict the effect of more packing beads on the role of restrikes, because several factors, e.g. also the alignment of the dielectric beads, can affect the discharge behavior, as revealed in [23]. We will further investigate this in our future work.

We have also simulated the discharge behavior without including dielectric layers covering both electrodes and by including only one dielectric layer covering the bottom electrode. Our results show that the general conclusions about the influence of the dielectric constant of the packing beads, such as the generation of local discharges at higher dielectric constant, remain the same.

4.4. Comparison with experimental observations

The predicted trends in discharge development in a packed bed DBD reactor for packing materials with rising dielectric constants are in qualitative agreement with our experimental observations of light emission. The measurements by fast-camera imaging for packings with different dielectric constants are presented in Fig. 8 and clearly show the transition of the dominant discharge pattern from surface discharges at $\varepsilon_r = 5$ (Fig. 8(a)) to local discharges at $\varepsilon_r = 2600$ (Fig. 8(d)). Indeed, at $\varepsilon_r = 5$ and 9 (Fig. 8(a) and (b)), the light emission is observed over a large region, corresponding to surface discharges covering most of the packing beads. Some local discharges at the contact points also exist, but they are not so apparent. At $\varepsilon_r = 25$, the plasma tends to ignite as a local discharge at the contact points, but the surface discharges are also visible on the bead surfaces (Fig. 8(c)). Both modes thus co-exist, in agreement with our simulations. At $\varepsilon_r = 2600$, intense plasma spots are observed at the contact points of the beads, corresponding to the local discharges, and no surface discharges are visible (Fig. 8(d)). Therefore, the plasma does not propagate on the surface of the $BaTiO_3$ beads. This trend is also in good agreement with recent experimental observations by Butterworth and Allen in a single pellet DBD reactor [42]. It is worth mentioning that the $BaTiO_3$ experiments were performed at a lower voltage of 7.5 kV, thus limiting the intensity of the microdischarges, because the pulsed voltage could not reach a higher value due to the large capacitance of the packed bed. In the supporting information, we provide images for the positive polarity, where the local microdischarges with $BaTiO_3$ packing are more intense, and thus more clearly visible (see Fig. S10). Moreover, as is well known, glass beads are transparent, so they are hard to capture clearly with the camera.

4.5. Propagation speed of streamers and surface ionization waves

Another important effect of the rising dielectric constant of the packing beads is the higher streamer propagation speed between the dielectric layer and the packing beads, as well as the higher propagation speed of the surface ionization waves on the surface of the dielectric layer or packing beads. In Fig. 9, we plot the time-averaged streamer propagation speed from the upper dielectric layer to the top dielectric bead (black line) and the propagation speed of the surface ionization wave from the central axis to a distance of 3 mm on the surface of the top dielectric layer (red line), as a function of the dielectric constant of the packing beads. When $\varepsilon_r = 5$, the streamer crosses the gap of 1.25 mm with a propagation speed of ca.3.1 $\times 10^5$ m/s, which corresponds to a time of 4 ns. This was indeed illustrated in Fig. 4. When $\varepsilon_r = 1000$, the speed increases to ca. 9.3 $\times 10^5$ m/s, corresponding to a time for crossing the gap of 1.3 ns (cf. Fig. 6). These propagation speeds are comparable to experimental measurements. For example, Briels et al. measured the propagation speeds of positive and negative streamers in air [51]. For an applied voltage of −30 kV in a 4 cm gap, they reported speeds of 5 $\times 10^5$ m/s. Overall, for voltages varying between 10 kV and 100 kV, the streamer speeds were between 2 $\times 10^5$ m/s and 4 $\times 10^6$ m/s.

Similarly, upon rising dielectric constant of the packing beads, the propagation speed of the surface ionization wave on the surface of the top dielectric layer increases, as a result of the stronger electric field near the edge of the surface ionization wave and hence the higher electron temperature, which leads to a larger electron impact ionization rate, as discussed above. It is clear from Fig. 9 that the propagation speeds of streamer and surface ionization wave are very similar to each other. The surface ionization wave seems to propagate a bit faster than the streamer for packing materials with $\varepsilon_r = 1000$, but the difference is probably not significant. Indeed, the two speeds correspond to different discharge mechanisms: the streamer propagation is dominated by the positive restrike process while the surface ionization wave is produced by surface charging, which creates electric field components parallel to

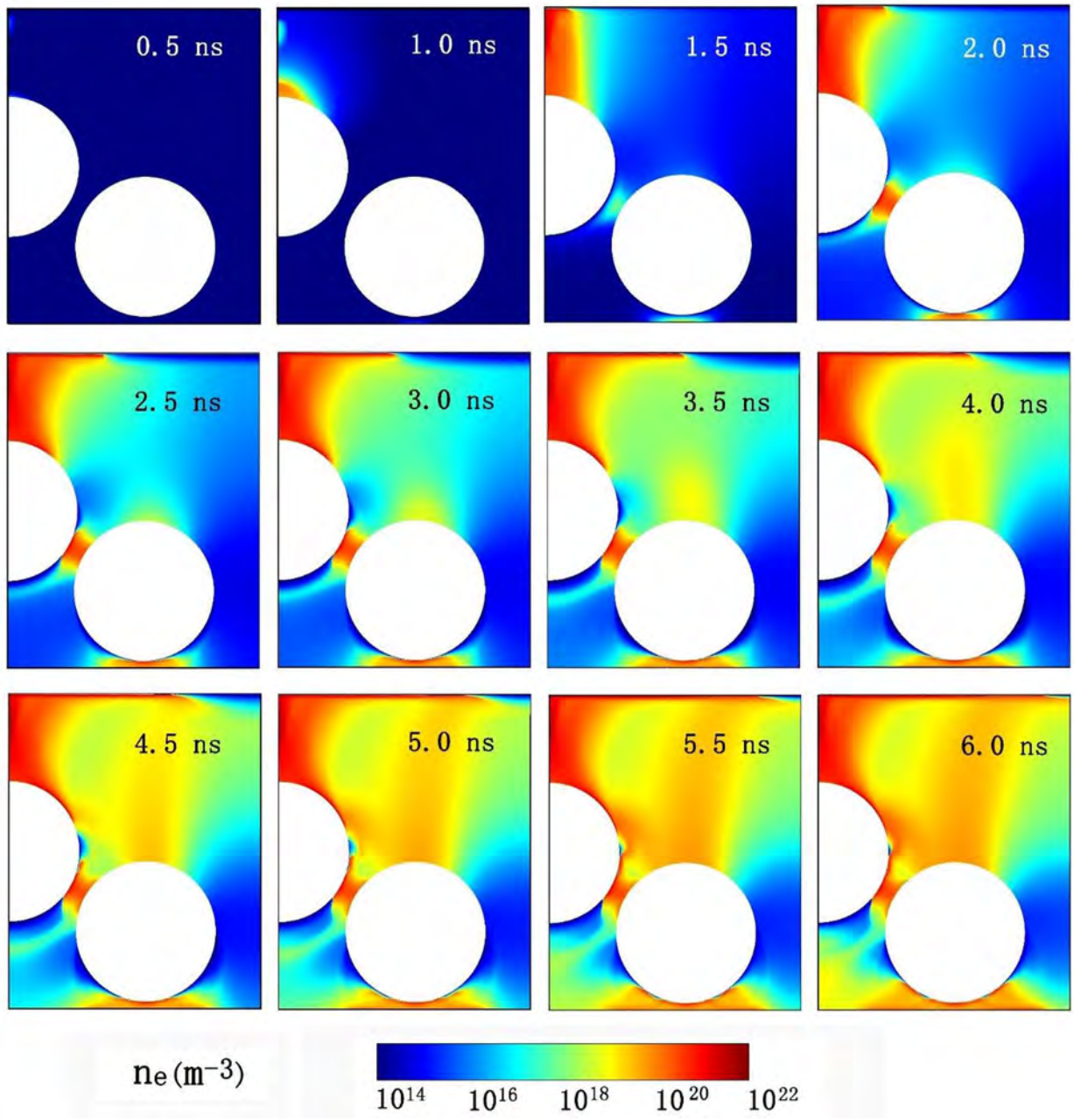

Fig. 7. Evolution of the electron density distribution over 6 ns, for a packing with ε_r = 100. The same behavior was also observed for ε_r = 9 and 25.

the dielectric surface. Note that no surface streamer propagation is observed on the packing beads with ε_r = 1000. The higher propagation speed of the surface ionization wave specifically applies to the surface of the top dielectric layer. It is worth mentioning that the propagation velocity described above is not for the surface ionization waves on the packing beads but on the dielectric layer surface because no surface discharge propagation takes place with a high dielectric constant of 1000.

In summary, our simulations show that packing beads with larger dielectric constants lead to a higher streamer propagation speed, and thus, a shorter time is needed to fully develop the discharge across the electrodes (cf. Figs. 4 and 6). This is in good agreement with experimental observations by Kim et al. [40].

4.6. Production of reactive species

Finally, the faster streamer propagation and discharge development with larger dielectric constant of the packing beads also leads to a faster production of reactive species, as clearly presented in Fig. 10. Indeed, as shown before, a larger dielectric constant of the packing beads results in a stronger electric field and hence a higher electron temperature (cf Figs. S1 and S6 in the SI) and thus a higher production rate of reactive species, such as oxygen and nitrogen atoms, by electron impact dissociation of the molecules.

Fig. 10 also illustrates that the volume-averaged number density of electrons is higher for ε_r = 1000 at t = 6 ns than for ε_r = 5 at t = 20 ns, i.e., when the discharge has fully developed across the electrodes in both cases. This is because of the stronger electric field and hence higher electron temperature at larger dielectric constant of the packing, causing more electron impact ionization. For the same reason, the volume-averaged number density of N atoms is also higher for ε_r = 1000, because of the higher electron impact dissociation rate of N_2 molecules. In contrast, the volume-averaged number density of O atoms and O_3 molecules is slightly lower for ε_r = 1000 than for ε_r = 5. This is due to

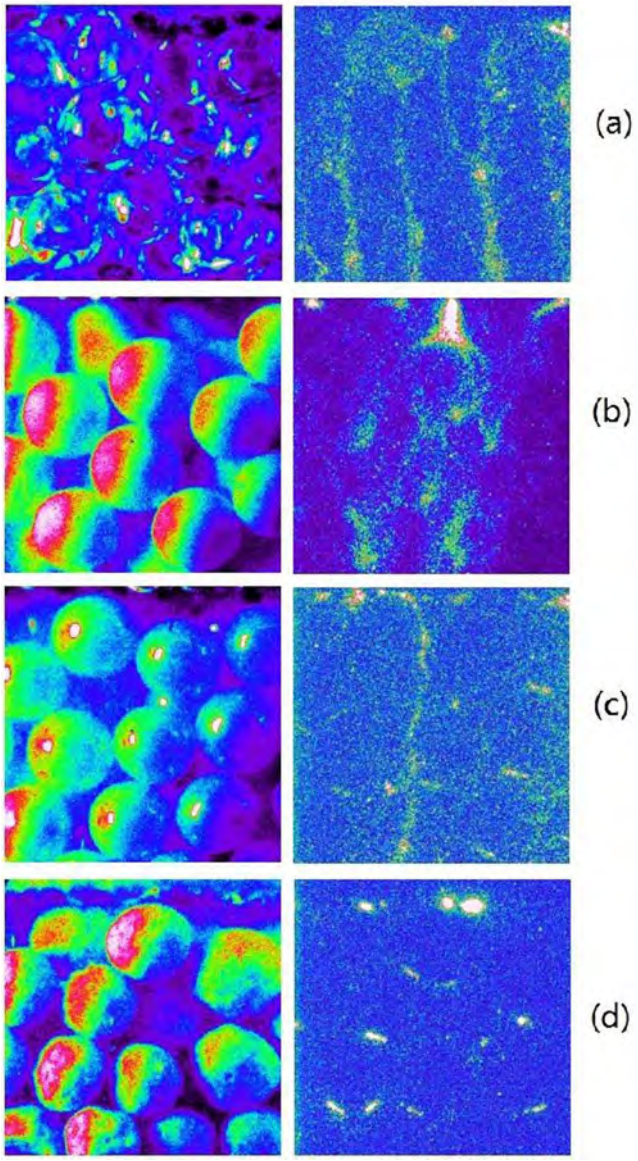

Fig. 8. Experimental imaging of the microdischarges in a packed bed reactor, with applied voltage of −10 kV, by fast ICCD camera imaging of the visible emission using a microscope lens and an observation gate width of 100 ns. (a) glass, ε_r = 5; (b) Alumina, ε_r = 9; (c) Zirconia, ε_r = 25; (d) $BaTiO_3$, ε_r = 2600. The left figures show the location of the packing beads without discharge, to better understand the right figures, which illustrate the images of discharge plasma. For $BaTiO_3$, a lower applied voltage of −7.5 kV was used, because the pulsed voltage could not reach a higher value due to the large capacitance of the packed bed. For glass, alumina and $BaTiO_3$, the dielectric constants are company guaranteed values. For the dielectric constant of zirconia, we use a typical value from literature. In [49], a range of 12–25 is reported, while Ref. [50] gives a value of 28.6. In our work, we use a typical value of 25.

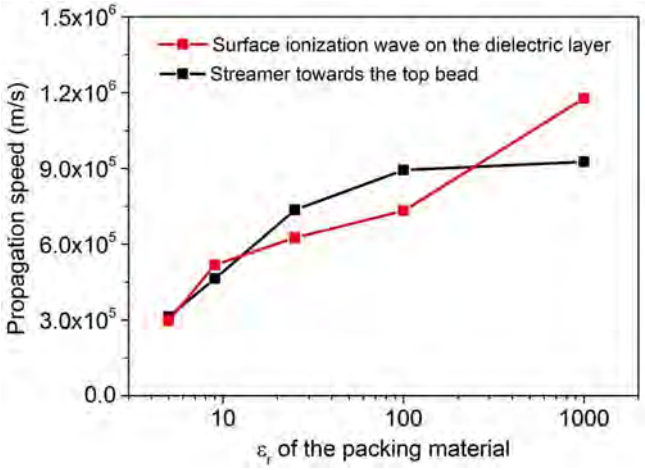

Fig. 9. Time-averaged streamer propagation speed from the upper dielectric layer to the top dielectric bead (black line) and propagation speed of the surface ionization wave from the central axis to a distance of 3 mm on the surface of the top dielectric layer (red line), as a function of dielectric constant of the packing. (For interpretation of the references to colour in this figure legend, the reader is referred to the web version of this article.)

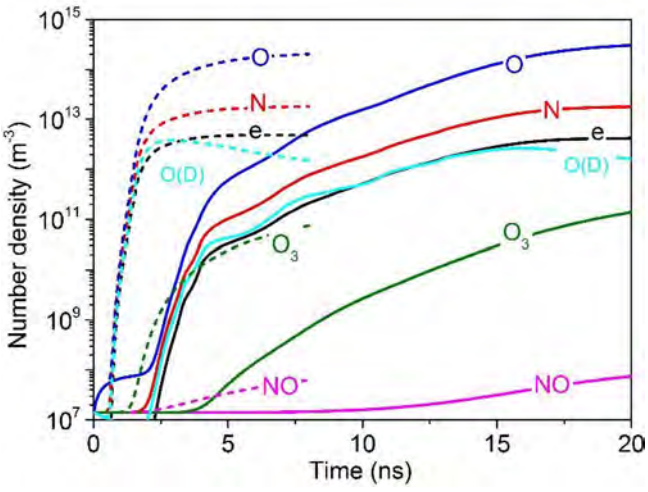

Fig. 10. Time evolution of the volume-averaged number density of reactive species for ε_r = 5 (solid lines) and ε_r = 1000 (dashed lines).

the lower fraction of electron energy transferred to the channel of O_2 dissociation, as a result of the higher reduced electric field (see Fig. S10 in the SI). The lower number density of O atoms also leads to a drop in the production rate of O_3 (Reactions R17 and R18 in the SI), explaining the lower volume-averaged number density of O_3 as well.

Our calculations reveal that the restrike channels, the surface discharges and the local discharges between the packing beads contribute significantly to the formation of reactive species, because of their higher electric field and hence higher electron temperatures, although the contribution from the standing filamentary microdischarges is also non-negligible. This is indicated for the net production rate of N atoms and O atoms for a packing with ε_r = 1000 in Fig. 11.

Indeed, at t = 1.0 ns, the highest production rate of N atoms and O atoms appears in the positive restrike channel, which has a higher electron temperature (cf Fig. S6 in the SI) and hence higher electron impact dissociation rate. The production rate of O atoms is higher than that of N atoms, because of the lower threshold level of electron impact dissociation (12.6 eV vs 15.6 eV).

At t = 1.5 ns, the production rates of N atoms and O atoms are also higher at the contact points between the packing beads, due to the local discharges in these regions. Furthermore, a surface ionization wave appears on the top dielectric layer at the same time instant, and a high production rate of both N atoms and O atoms occurs near the edge of this surface ionization wave and propagates outwards.

With the discharge development, plasma continuously charges the dielectrics, and thus the electric field as well as the electron temperature inside the stable filamentary microdischarge channel between the top dielectric layer and the left bead gradually drops (cf Fig. S6 in the SI). As a result, the production rate of N atoms and O atoms, which is mainly by electron impact dissociation, decreases. Note that the electron impact dissociation rate of N_2 (cf Fig. S11 in the SI) and hence the production rate of N atoms is more sensitive to the decreasing electron energy, due to the higher threshold energy compared with that of O

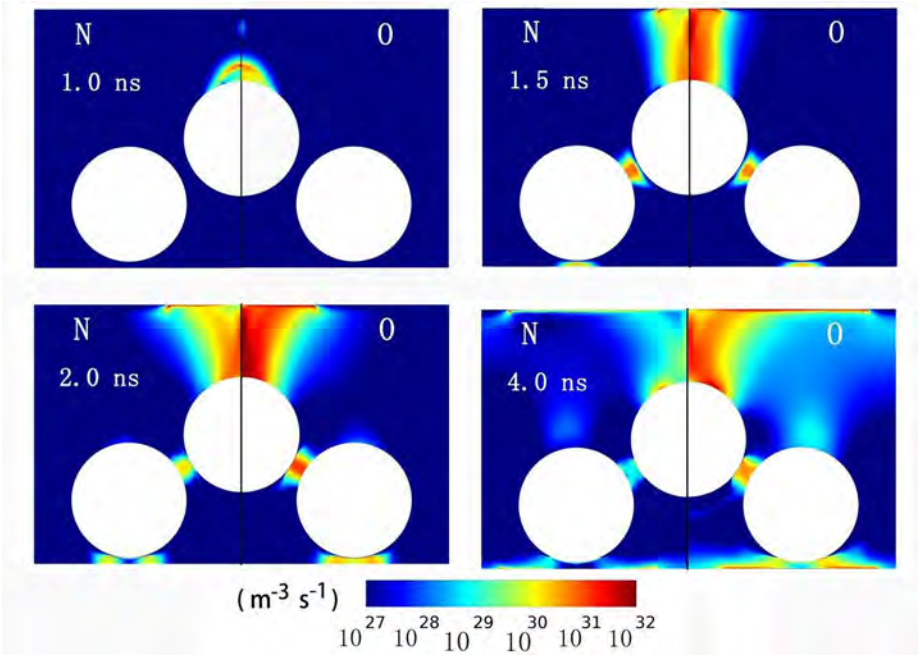

Fig. 11. Distribution of the net production rate of N atoms (left) and O atoms (right) at t = 1.0 ns, 1.5 ns, 2.0 ns and 4.0 ns, for a packing with ε_r = 1000.

atoms. This leads to a more drastic drop in the production rate of N atoms inside the filamentary microdischarge (see Fig. 11; 2.0 ns and 4.0 ns). As a result, the highest production rate of N atoms in the central filamentary discharge channel between the top dielectric layer and the top surface of the left bead is more than two orders of magnitude lower than the maximum production rate in the surface ionization wave on the surface of the top dielectric layer at 4.0 ns (1.0×10^{30} $m^{-3}s^{-1}$ vs 5.5×10^{32} $m^{-3}s^{-1}$). In contrast, the maximum production rate of O atoms in the filamentary discharge is only one order of magnitude lower than in the surface ionization wave (2.8×10^{31} $m^{-3}s^{-1}$ vs 3.2×10^{32} $m^{-3}s^{-1}$), indicating that the standing filamentary microdischarge still has a significant contribution to the production of O atoms, mainly because it occupies a relatively large volume.

4.7. Consequences for environmental applications of packed bed DBD reactors

Our study indicates that packing materials with different dielectric constants significantly influence the plasma characteristics, which will definitely affect the performance of packed bed reactors for environmental applications, such as ozone generation, gaseous pollutant removal or greenhouse gas conversion [52].

For example, our simulations show that for a packing with large dielectric constant, the O_3 concentration is somewhat lower than for a packing with smaller dielectric constant, because of the lower electron impact dissociation of O_2 towards O and hence the lower production rate of O_3. This is due to the enhanced electric field and mean electron energy, as discussed in previous section. Hence, for ozone generation, the electric field must be controlled in a moderate range, by choosing a packing with moderate dielectric constant. This has been confirmed in various experimental studies [53–55]. Furthermore, a packing with high dielectric constant leads to a higher electron number density at the contact points between the beads and this may lead to local heating near the contact points, which may promote the destruction of O_3 via thermal dissociation (Reaction R13 in the SI). A similar explanation was also proposed by Yamamoto et al. [55] to interpret the results of Ogata et al. [56].

For gaseous pollutant removal, a packing with higher dielectric constant may increase the performance, because of the enhanced electric field and hence higher electron temperature, as predicted by our model, and this may enhance the destruction of gaseous pollutants. For example, Ogata et al. [56] employed ferroelectric pellets with dielectric constant ranging from 20 to 15,000, to investigate their influence on the performance for benzene removal, and reported that the benzene removal efficiency increases with rising dielectric constant at a fixed input power. However, rising the dielectric constant of the packing beads cannot unlimitedly improve the energy efficiency for pollutant removal, although higher dielectric constants are still favorable from engineering viewpoint, because the discharge power can be enhanced upon increasing the dielectric constant of the packing at the same applied voltage [53]. A similar trend, i.e. higher dielectric constants giving rise to a higher conversion efficiency, is found for the decomposition of CO_2 in a dielectric packed bed plasma reactor [14,57,58].

Additionally, both our simulations and experiments reveal that in case of higher dielectric constant of the packing, the local discharges gradually dominate over surface streamers. Butterworth and Allen concluded that the local (or partial) discharge mode is characterized by the absence of conductive charge transfer between the DBD electrodes [42]. They only observed plasma formation between the electrodes and the poles of the bead in their single catalyst bead DBD reactor in case of a $BaTiO_3$ packing. Indeed, beads with higher dielectric constant have a greater capacity to trap charges, limiting the extent of plasma formation in the reactor. This is in good agreement with our results. This may have implications for the efficiency of plasma catalytic gas treatment, because the catalyst activation may be limited by constraining the discharge to the contact points of the beads [42]. Indeed, in [59] a lower dielectric constant of the packing yielded a higher toluene removal efficiency, and this was attributed to the limited plasma volume with higher dielectric constant ($BaTiO_3$, ε_r = 15,000) compared with lower dielectric constant ($SrTiO_3$, ε_r = 330). However, the morphology, porosity and chemical activity (acid-base properties) of the packing material may also affect the removal efficiency.

Which effect will be dominant at higher dielectric constants, i.e., (i) the more pronounced electric field enhancement and thus higher electron temperature and density, yielding more production of reactive species, or (ii) the confined discharge near the contact points, limiting the catalyst activation, will depend on other conditions as well, such as the applied power, frequency, gas flow rate, discharge gap and bead size. Moreover, other material properties, such as porosity, may also

influence the plasma characteristics and the performance, besides the dielectric constants of the packing beads. Indeed, recent experiments for CO_2 conversion showed that the conversion and energy efficiency sometimes rise upon higher dielectric constant of the packing beads, but the best results are not always reached for the highest dielectric constant, indicating that more effects play a role [14].

5. Conclusion

In this paper, we investigated the propagation of a streamer in a packed bed DBD reactor operating in dry air, and more specifically its behavior when it finds a dielectric packing on its path towards the opposite electrode. For these calculations, photoionization was included by means of the Helmholtz equations, to correctly simulate the streamer propagation.

Our calculations predict that the plasma formation in a packed bed DBD reactor in dry air may exhibit three types of discharge behavior, i.e., positive restrikes, filamentary microdischarges, also localized between the packing beads, and surface ionization waves, in agreement with literature [23,36–40]. Positive restrikes between the dielectrics result in the formation of filamentary microdischarges. Surface charging creates electric field components parallel to the dielectric surface, and leads to the formation of surface ionization waves. For a low dielectric constant of the packing ($\varepsilon_r = 5$), plasma ignition between the beads occurs directly in the mode of surface discharges (or surface ionization waves), which can connect with the surface of the adjacent bead, while for a high dielectric constant ($\varepsilon_r = 1000$), no surface streamer jumping towards the adjacent bead surface is observed and spatially limited filamentary microdischarges, so-called local discharges, are generated between the beads. For intermediate dielectric constants, a mixed mode of surface discharges and local discharges exists. The local discharges first appear at the contact points of the packing beads and they promote the propagation of the surface discharges towards the next packing bead.

The positive restrikes, local discharges and surface discharges contribute significantly to the production of reactive species. These discharge modes indeed exhibit an enhanced electric field and hence they create a burst of energetic electrons, which cause the production of reactive species by electron impact dissociation of the molecules, in spite of the small volume they occupy. Our simulations reveal that a higher dielectric constant of the packing leads to a higher volume-average number density of N atoms and electrons, but a somewhat lower concentration of O atoms and O_3 molecules, indicating that the packing with most suitable dielectric constant depends on the application. For gaseous pollutant abatement, raising the dielectric constant will generally be beneficial, as a result of the enhanced electric field and hence a higher pollutant destruction rate. However, for ozone generation, the electric field enhancement must be controlled, by using a packing with moderate dielectric constant.

Our results also show that a higher dielectric constant constrains the discharge to the contact points of the beads, regardless of their contribution to the electric field enhancement. This may limit the catalyst activation due to the limited catalyst surface area in contact with the discharge, and thus it may have implications for the efficiency of plasma catalytic gas treatment. Therefore, the best results for gaseous pollutant abatement are not always reached for the highest dielectric constant [59].

In plasma catalysis, packing beads with different dielectric constants are typically used as supports for the catalytic materials. Therefore, this study is important to gain a better insight in how different packing materials can influence the performance of packed bed DBD reactors for environmental applications

Acknowledgments

We acknowledge financial support from the Fund for Scientific Research Flanders (FWO) (grant nos G.0217.14 N, G.0254.14 N and G.0383.16 N), the TOP-BOF project of the University of Antwerp, the European Marie Skłodowska-Curie Individual Fellowship “GlidArc” within Horizon2020 (Grant No. 657304) and the Institute for the Promotion of Innovation by Science and Technology in Flanders (IWT Flanders). This research was carried out in the framework of the network on Physical Chemistry of Plasma-Surface Interactions – Interuniversity Attraction Poles, phase VII (http://psi-iap7.ulb.ac.be/), and supported by the Belgian Science Policy Office (BELSPO). The calculations were carried out using the Turing HPC infrastructure at the CalcUA core facility of the Universiteit Antwerpen (UAntwerpen), a division of the Flemish Supercomputer Center VSC, funded by the Hercules Foundation, the Flemish Government (department EWI) and the UAntwerpen.

Appendix A. Supplementary data

Supplementary data associated with this article can be found, in the online version, at http://dx.doi.org/10.1016/j.cej.2017.11.139.

References

[1] E.C. Neyts, K. Ostrikov, M.K. Sunkara, A. Bogaerts, Chem. Rev. 115 (2015) 13408–13446.
[2] A. Ogata, H. Einaga, H. Kabashima, S. Futamura, S. Kushiyama, H.H. Kim, Appl. Cat. B: Environ. 46 (2003) 87–95.
[3] A. Gómez-Ramírez, A.M. Montoro-Damas, M.A. Rodríguez, A.R. González-Elipe, J. Cotrino, Chem. Eng. J. 314 (2017) 311–319.
[4] X. Tu, H.J. Gallon, J.C. Whitehead, IEEE Trans. Plasma Sci. 39 (2011) 2172.
[5] Ch. Subrahmanyam, M. Magureanu, A. Renken, L. Kiwi-Minsker, Appl. Catal. B: Environ. 65 (2006) 150.
[6] F. Holzer, U. Roland, F.-D. Kopinke, Appl. Catal. B: Environ. 38 (2002) 163–181.
[7] S.J. Xu, J.C. Whitehead, P.A. Martin, Chem. Eng. J. 327 (2017) 764–773.
[8] T. Nozaki, K. Okazaki, Catal. Today 211 (2013) 29–38.
[9] A. Maciuca, C. Batiot-Dupeyrat, J.M. Tatibouët, Appl. Catal. B: Environ. 125 (2012) 432–438.
[10] K. Van Laer, A. Bogaerts, Energy Technology 3 (2015) 1038–1044.
[11] D.H. Mei, X.B. Zhu, C.F. Wu, B. Ashford, P.T. Williams, X. Tu, Appl. Cat. B: Environ. 182 (2016) 525–532.
[12] T. Butterworth, R. Elder, R. Allen, Chem. Eng. J. 293 (2016) 55–67.
[13] X. Tu, J.C. Whitehead, Appl. Cat. B: Environ. 125 (2012) 439–448.
[14] I. Michielsen, Y. Uytdenhouwen, J. Pype, B. Michielsen, J. Mertens, F. Reniers, V. Meynen, A. Bogaerts, Chem. Eng. J. 326 (2017) 477–488.
[15] A.I. Pylinina, I.I. Mikhalenko, Theor. Exp. Chem. 49 (2013) 65.
[16] V. Demidyuk, J.C. Whitehead, Plasma Chem. Plasma Process. 27 (2007) 85.
[17] A. Rousseau, O. Guaitella, J. Ropcke, L.V. Gatilova, Y.A. Tolmachev, Appl. Phys. Lett. 85 (2004) 2199.
[18] J.S. Chang, K.G. Kostov, K. Urashima, T. Yamamoto, Y. Okayasu, T. Kato, T. Iwaizumi, K. Yoshimura, IEEE Trans. Ind. Appl. 36 (2000) 1251.
[19] K. Takaki, J.S. Chang, K.G. Kostov, IEEET Dielect El. In. 11 (2004) 481.
[20] W.S. Kang, J.M. Park, Y. Kim, S.H. Hong, IEEE Trans. Plasma Sci. 31 (2003) 504.
[21] H. Russ, M. Neiger, J.E. Lang, IEEE Trans. Plasma Sci. 27 (1999) 38.
[22] N.Y. Babaeva, M.J. Kushner, Plasma Sources Sci. Technol. 18 (2009) 035009.
[23] J. Kruszelnicki, K.W. Engeling, J.E. Foster, Z. Xiong, M.J. Kushner, J. Phys. D: Appl. Phys. 50 (2017) 025203.
[24] Y. Zhang, H. Wang, W. Jiang, A. Bogaerts, New J. Phys. 17 (2015) 083056.
[25] K. Van Laer, A. Bogaerts, Plasma Sources Sci. Technol. 25 (2016) 015002.
[26] K. Van Laer, A. Bogaerts, Plasma Process. Polym. 14 (2017) e1600129.
[27] K. Van Laer and A. Bogaerts, Plasma Sources Sci. Technol. (submitted).
[28] Q. Ye, T. Zhang, F. Lu, J. Li, Z. He, F. Lin, J. Phys. D: Appl. Phys. 41 (2008) 025207.
[29] A. Bourdon, V.P. Pasko, N.Y. Liu, S. Célestin, P. Ségur, E. Marode, Plasma Sources Sci. Technol. 16 (2007) 656–678.
[30] A. Luque, U. Ebert, C. Montijn, W. Hundsdorfer, Appl. Phys. Lett. 90 (2007) 081501.
[31] G. Steinle, D. Neundorf, W. Hiller, M. Pietralla, J. Phys. D: Appl. Phys. 32 (1999) 1350–1356.
[32] U. Ebert, W. van Saarloos, C. Caroli, Physial Review E 55 (1997) 1530–1549.
[33] L. Papageorghiou, E. Panousis, J.F. Loiseau, N. Spyrou, B. Held, J. Phys. D: Appl. Phys. 42 (2009) 105201.
[34] N.Y. Babaeva, A.N. Bohj, M.J. Kushner, Plasma Sources Sci. Technol. 15 (2006) 591–602.
[35] N.Y. Babaeva, M.J. Kushner, Plasma Sources Sci. Technol. 20 (2011) 035009.
[36] H.H. Kim, A. Ogata, Eur. Phys. J. Appl. Phys. 55 (2011) 13806.
[37] H.H. Kim, J.H. Kim, A. Ogata, J. Phys. D: Appl. Phys. 42 (2009) 135210.
[38] H.H. Kim, Y. Teramoto, N. Negishi, A. Ogata, Catalysis Today 256 (2015) 13–22.
[39] H.H. Kim, Y. Teramoto, T. Sano, N. Negishi, A. Ogata, Appl. Catalysis B: Environ. 166–167 (2015) 9–17.
[40] H.H. Kim, Y. Teramoto, A. Ogata, J. Phys. D: Appl. Phys. 49 (2016) 459501.
[41] X. Tu, H.J. Gallon, M.V. Twigg, P.A. Gorry, J.C. Whitehead, J. Phys. D: Appl. Phys.

44 (2011) 274007.
[42] T. Butterworth, R.W.K. Allen, Plasma Sources Sci. Technol. 26 (2017) 065008.
[43] J.C. Whitehead, J. Phys. D: Appl. Phys. 49 (2016) 243001.
[44] http://www.comsol.com.
[45] A. Ogata, K. Miyamae, K. Mizuno, S. Kushiyama, M. Tezuka, Plasma Chem. Plasma Process. 22 (2002) 537.
[46] P. Rajasekaran, P. Mertmann, N. Bibinov, D. Wandke, W. Viöl, P. Awakowicz, Plasma Process. Polym. 7 (2010) 665–675.
[47] D. Nelson, M. Benhenni, O. Eichwald, M. Yousfi, J. Appl. Phys. 94 (2003) 96–103.
[48] N.Y. Babaeva, M.J. Kushner, Plasma Sources Sci. Technol. 23 (2014) 065047.
[49] P.J. Harrop, J.N. Wanklyn, Br. J. Appl. Phys. 18 (1967) 739–742.
[50] M.A. Subramanian, R.D. Shannon, Mat. Res. Bullet. 24 (1989) 1477–1483.
[51] T.M.P. Briels, J. Kos, G.J.J. Winands, E.M. van Veldhuizen, U. Ebert, J. Phys. D: Appl. Phys. 41 (2008) 234004.
[52] H.L. Chen, H.M. Lee, S.H. Chen, M.B. Chang, Ind. Eng. Chem. Res. 47 (2008) 2122–2130.
[53] F. Holzer, F.D. Kopinke, U. Roland, Plasma Chem. Plasma Process. 25 (2005) 595.
[54] J.D. Moon, S.T. Geum, I.E.E.E. Trans, Ind. Appl. 34 (1998) 1206.
[55] T. Yamamoto, J.S. Chang, A.A. Berezin, H. Kohno, S. Honda, A. Shibuya, J. Adv. Oxid. Technol. 1 (1996) 67.
[56] A. Ogata, N. Shintani, K. Mizono, S. Kushiyama, T. Yamamoto, IEEE Trans. Ind. Appl. 35 (1999) 753.
[57] Q. Yu, M. Kong, T. Liu, J. Fei, X. Zheng, Plasma Chem. Plasma Process. 32 (2012) 153–163.
[58] X. Duan, Z. Hu, Y. Li, B. Wang, AIChE J. 61 (2015) 898–903.
[59] H. Arai, A. Ogata, A. Yamasaki, H.H. Kim, Y. Yanagisawa, Kagaku Kogaku Ronbunshu 36 (2010) 310–316 in Japanese.